and the characteristic equation is given by

$$(\alpha_1\alpha_2 - \beta_x^2)\sin\beta_x d + (\alpha_1 + \alpha_2)\beta_x \cdot \cos\beta_x d = 0 \quad \text{(A.3)}$$

where

$$\alpha_1 = (\beta_z^2 - k_1^2)^{1/2} > 0 \qquad \alpha_2 = (\beta_z^2 - k_2^2)^{1/2} > 0.$$

For the TM-modes group, the field components in an anisotropic dielectric slab are expressed as

$$H_z = 0$$

$$E_z = \frac{\omega\mu}{\beta_z}\{A\cos\beta_x x + B\sin\beta_x x\}$$

$$H_y = b\{jA\sin\beta_x x - jB\cos\beta_x x\}$$

$$E_y = 0 \quad \text{(A.4)}$$

where

$$b = \frac{k_{zz}^2}{\beta_x\beta_z} \qquad \beta_x^2 = k_{zz}^2 - \frac{k_{zz}^2}{k_{xx}^2}\beta_z^2$$

and the characteristic equation is given by

$$\left(\alpha_1\alpha_2 - \frac{k_1^2k_2^2}{k_{zz}^4}\beta_x^2\right)\sin\beta_x d + \left(\frac{k_2^2}{k_{zz}^2}\alpha_1 + \frac{k_1^2}{k_{zz}^2}\alpha_2\right)\beta_x \cdot\cos\beta_x d = 0 \quad \text{(A.5)}$$

where

$$\alpha_1 = (\beta_z^2 - k_1^2)^{1/2} > 0 \qquad \alpha_2 = (\beta_z^2 - k_2^2)^{1/2} > 0.$$

References

[1] H. Unz, "Propagation in arbitrarily magnetized ferrites between two conducting parallel planes," *IEEE Trans. Microwave Theory Tech.*, vol. MTT-11, pp. 204–210, May 1963.

[2] S. Wang, M. L. Shah, and J. D. Crow, "Wave propagation in thin-film optical waveguides using gyrotropic and anisotropic materials as substrates," *IEEE J. Quantum Electron. (Part II: Special Issue on 1971 IEEE/OSA Conference on Laser Engineering and Applications)*, vol. QE-8, pp. 212–216, Feb. 1972.

[3] D. F. Nelson and J. McKenna, "Electromagnetic modes of anisotropic dielectric waveguides at p-n junctions," *J. Appl. Phys.*, vol. 38, pp. 4057–4074, Sept. 1967.

[4] R. A. Andrews, "Crystal symmetry effects on nonlinear optical processes in optical waveguides," *IEEE J. Quantum Electron.*, vol. QE-7, pp. 523–529, Nov. 1971.

[5] J. A. Stratton, *Electromagnetic Theory*. New York: McGraw-Hill, 1941, p. 362.

Electromagnetic-Wave Propagation in the Shielded Ring Line

YVES GARAULT AND CLAUDE FRAY

Abstract—**A theoretical analysis is presented of a periodic structure consisting of equally spaced perfectly conducting rings. The dispersion relation satisfied by the different modes of the shielded ring line is determined. This analysis shows that cylindrically symmetric modes identical with those of smooth guides and hybrid modes can travel in this periodical structure.**

The asymptotic values of the dispersion relation show the different properties of these hybrid modes. The EH_{n1} modes can be slow, fast, or can travel at light velocity according to the frequency. The EH_{nq} ($q > 1$) modes are fast modes and exchange their cutoff frequencies for particular values of the geometrical parameters of the structure.

These theoretical predictions are verified experimentally by recording the dispersion characteristics of the first modes.

For deflecting radio-frequency structures, the fundamental EH_{11} mode is interesting. This deflection constant is measured on a $\pi/2$ wave structure.

I. Introduction

IN THE SETTING of a research of waveguide structures for RF separators of ultrarelativistic particles, we studied the shielded ring line in which the fundamental hybrid mode is a very interesting deflector mode. In order to study this structure, we followed the same method that Pierce and Field [1] utilized to investigate the propagation of surface waves on the helix. Pierce assumed the helix to be an ideal cylinder with conduction in the helical direction only (the "sheath" helix). The space harmonic fields are then neglected. A more satisfying approach called the "tape" helix was given by Sensiper [2]. He assumed the helix to be wound to an infinitely thin conducting tape and took the electric field at the center line of the tape to be zero. In other respects, he studied a limiting case of the helix: the open ring line composed of equally spaced perfectly conducting rings.

The surface waves which travel along this open ring line are slow waves ($v_p < c$). In the Brillouin diagram $\omega = f(\beta)$ connecting the wave frequency to the phase constant β, the dispersion characteristics of modes are only to be found in the slow-wave domain. If we surround this line with a conducting pipe, the modes can be fast and the dispersion characteristic intersects the straight line $v_p = c$ and is carried on into the fast-wave domain. We have developed the partial study of Falnes [3] on the different modes of this structure.

Manuscript received March 23, 1973; revised August 1, 1973.
The authors are with the Faculty of Sciences, Microwave Electronics Laboratory, University of Limoges, Limoges, France.

These modes which can travel at light velocity are hybrid EH modes (E_z,$H_z \neq 0$). When the velocity is very close to c, only certain hybrid EH solutions provide a deflecting force that is not negligibly small. In cylindrical coordinates, the modes with angular symmetry of first order in θ are EH deflection modes, and the deflecting force is practically free of aberrations when $v_p \simeq c$. Here we generally study the hybrid EH modes of n-fold symmetry in θ which travel into the shielded ring line and examine the modes with angular symmetry of first order in θ in greater detail. Finally, we measure the deflection constant for a shielded ring waveguide operating in the fundamental mode at 3 GHz.

II. Properties of Guided Waves Parallel to the $0z$ Axis

The electromagnetic field of a wave traveling without attenuation in the direction of the z axis can be written in the form

$$\mathcal{E} = (\mathbf{E}_t + E_z\boldsymbol{u}) \exp j(\omega t - \beta z) \tag{1}$$

$$\mathcal{H} = (\mathbf{H}_t + H_z\boldsymbol{u}) \exp j(\omega t - \beta z) \tag{2}$$

where $\mathbf{E}_t$,$\mathbf{H}_t$ and E_z,H_z, are, respectively, the projections of $\mathcal{E}$ and $\mathcal{H}$ on a transverse plane perpendicular to $0z$ and on this axis of unit vector $\boldsymbol{u}$; $\beta = \omega/v_p$ is the phase constant.

By introducing $\mathcal{E}$ and $\mathcal{H}$ into Maxwell's equation, we deduce the relation [4]

$$k_c^2\mathbf{E}_t = j[kZ(\boldsymbol{u} \times \nabla_\perp H_z) - \beta\nabla_\perp E_z] \tag{3}$$

$$k_c^2\mathbf{H}_t = -j[k/Z(\boldsymbol{u} \times \nabla_\perp E_z) + \beta\nabla_\perp H_z] \tag{4}$$

$$\nabla_\perp^2 \begin{pmatrix} E_z \\ H_z \end{pmatrix} + k_c^2 \begin{pmatrix} E_z \\ H_z \end{pmatrix} = 0. \tag{5}$$

Here $k = \omega(\epsilon\mu)^{1/2} = \omega/c$ is the wavenumber for plane uniform waves, $k_c^2 = k^2 - \beta^2$ is the cutoff wavenumber, and $Z = (\mu/\epsilon)^{1/2}$ is the wave impedance of the medium. The relations (3) and (4) express the transverse components in terms of the longitudinal components, provided $v_p \neq c$; the latter are solutions of the scalar wave equations.

At $v_p = c$, both E_z and H_z components can exist and satisfy the relation [5]

$$Z(\boldsymbol{u} \times \nabla_\perp H_z) = \nabla_\perp E_z. \tag{6}$$

Then (3) and (4) are compatible.

This hybrid wave satisfying (6) at $v_p = c$ is an "EH" wave (E_z,$H_z \neq 0$) [5]. These hybrid waves are traveling in waveguides of heterogeneous structures and in periodic waveguides as the through periodic waveguides [6], the iris-loaded waveguide [7], and also, precisely, the shielded ring line.

We are lead to use solutions of (5) that are continuous for any phase velocity. In the cylindrical coordinates (r,θ,z) the longitudinal components can be expressed in the form [omitting the time factor exp ($j\omega t - \beta z$)] at $v_p \neq c$:

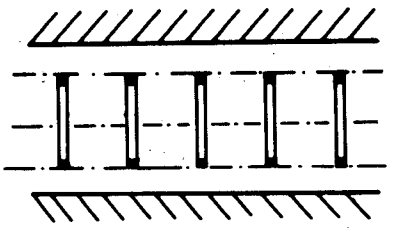

Fig. 1.

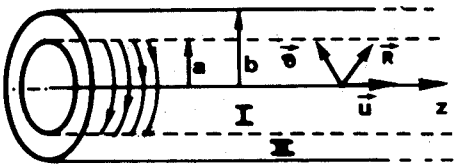

Fig. 2. The characters with arrows over them appear boldface in the text.

$$\begin{pmatrix} E_z \\ H_z \end{pmatrix} = \left\{ \begin{pmatrix} E_0 \\ H_0 \end{pmatrix} J_n^0(\chi_c,\rho) + \begin{pmatrix} E_1 \\ H_1 \end{pmatrix} N_n^0(\chi_c,\rho) \right\} \begin{pmatrix} \cos n\theta \\ \sin n\theta \end{pmatrix}$$

where n is a positive integer which characterizes the symmetry in θ of the different modes; $J_n^0(\chi_c,\rho)$ and $N_n^0(\chi_c,\rho)$ are modified forms of Bessel functions [5, appendix II, pp. 296, 300] that are correct for any value of v_p. These solutions are given by making the following transformation $k_c r = \chi_c k r = \chi_c \rho$ in (5). It can be shown that

$$J_n^0(\chi_c,\rho) = \chi_c^{-n} J_n(\chi_c\rho)$$

$$N_n^0(\chi_c,\rho) = \chi_c^n(2 \log \chi_c J_n(\chi_c\rho) - \pi N_n(\chi_c\rho))$$

where $J_n(\chi_c\rho)$ and $N_n(\chi_c\rho)$ are trigonometric Bessel functions of the first and second kinds.

III. Dispersion Relations Satisfied by the Different Modes of the Shielded Ring Line

In order to simplify the analysis, we replace the real periodic ring line (Fig. 1) by a nonperiodic sheath which can conduct only in the ring direction (Fig. 2). This analysis gives satisfactory results, provided that the periodicity of the real structure is small compared with the wavelength.

Since it is not possible to solve (3) and (4) directly we are forced to decompose this structure into the two regions in which we can express the field components.

In the axial zone of diameter $2a$ in Fig. 2 (diameter of the continuous anisotropic surface), the components remain finite on axis and are then independent of $N_n^0(\chi_c,\rho)$. In the coaxial zone of inner diameter $2a$ and outer diameter $2b$, the EH waves satisfy for $r = b$ the boundary conditions of both TE and TM waves of smooth guides:

$$E_z(kb,\theta) = \frac{\partial H_z}{\partial \rho}(kb,\theta) = 0.$$

The most general EH wave, for $v_p \neq c$, has longitudinal fields of the form:

1) axial zone:

$$\begin{pmatrix} E_z^{I} \\ H_z^{I} \end{pmatrix} = \begin{pmatrix} E^{I} \\ H^{I} \end{pmatrix} J_n^0(\chi_c,\rho) \begin{pmatrix} \cos n\theta \\ \sin n\theta \end{pmatrix}$$

2) coaxial zone:

$$E_z^{II} = E^{II} Y_n^0(\chi_c,\rho) \cos n\theta$$

$$H_z^{II} = H^{II} Z_n^0(\chi_c,\rho) \sin n\theta$$

with

$$Y_n^0(\chi_c,\rho) = N_n^0(\chi_c,kb) J_n^0(\chi_c,\rho) - N_n^0(\chi_c,\rho) J_n^0(\chi_c,kb)$$

$$Z_n^0(\chi_c,\rho) = N_n^{0\prime}(\chi_c,kb) J_n^0(\chi_c,\rho) - N_n^0(\chi_c,\rho) J_n^{0\prime}(\chi_c,kb).$$

The transverse components of the two regions are deduced from the longitudinal components with the aid of (3) and (4).

Over the common surface, the tangential components of both regions must be continuous. The equivalent boundary conditions are for $r = a$

$$E_z^{I} = E_z^{II} \qquad E_\theta^{I} = E_\theta^{II} = 0 \qquad H_\theta^{I} = H_\theta^{II}.$$

We obtain a homogeneous system of linear equations. A nontrivial solution exists only if the determinant of the system is zero. The dispersion relation is determined from the equation resulting from the requirement that the determinant vanishes. By solving directly and simplifying by χ_c^2, we obtain at $v_p \neq c$

$$\frac{\beta^2}{k^2}\left(\frac{n}{ka}\right)^2 J_n^0(\chi_c,ka) J_n^{0\prime}(\chi_c,kb)\, Y_n^0(\chi_c,ka) + J_n^{0\prime}(\chi_c,ka) J_n^0(\chi_c,kb) Z_n^{0\prime}(\chi_c,ka) = 0. \quad (7)$$

At $v_p = c$, the dispersion relation collapses into an indeterminate form. To obtain the proper expression it is only necessary to transform (7) in such a way that χ_c^2 appears as a factor and to substitute the modified Bessel functions by their expressions when $v_p = c$ [9]. If we simplify by $n \neq 0$, $ka \neq 0$, and introduce $p = b/a$, we obtain

$$\frac{2}{(ka)^2} = 1 + 2\frac{p \log p}{p - p^{-1}}, \qquad n = 1 \quad (8)$$

$$\frac{2n}{(ka)^2} = \frac{1 - p^2}{n+1} - \frac{p}{p^{-n} - p^n} \cdot \left\{ \frac{p^{n+1} - p^{-(n+1)}}{n+1} + \frac{p^{n-1} - p^{1-n}}{n-1} \right\}, \qquad n \geq 2. \quad (9)$$

These expressions show that only one hybrid wave travels along the shielded ring line for each value of $n \neq 0$, at $v_p = c$.

IV. Analysis of the Dispersion Relation

A. The Special Case of Cylindrical Symmetry, $n = 0$

In this case, in which the fields are independent of θ, the dispersion relation (7) becomes

$$J_0'(k_c a) J_0(k_c b) Z_0'(k_c a) = 0. \quad (10)$$

These modes are modes of smooth guides that, with our approximation, are unperturbed by the rings. They correspond to:

1) the TM_{0q} modes of a smooth guide of diameter $2b$;
2) the TE_{0q} modes of a smooth guide of diameter $2a$;
3) the TE_{0q} coaxial modes of a coaxial guide (a,b).

B. Study of Dispersion Relation at Cutoff

The phase velocity of the modes is infinite at cutoff; β is zero and $\chi_c^2 = 1 - \beta^2/k^2$ is equal to unity. The dispersion relation takes the simple form

$$J_n(kb) J_n'(ka) Z_n'(ka) = 0. \quad (11)$$

At cutoff, the structure of the hybrid modes is the same as: 1) the TM_{nq} modes of the smooth guide of diameter $2b$ when kb is equal to one of the y_n^i roots of $J_n(kb)$; 2) the TE_{nq} modes of the smooth guide of diameter $2a$ when ka is equal to one of the x_n^j roots of $J_n'(ka)$; 3) the TE_{nq} coaxial modes of the coaxial guide (a,b) when ka is equal to one of the z_n^v roots of $Z_n'(ka)$.

When $p = b/a$ varies from infinity to unity; the EH_{nq} modes (qth mode of n-fold symmetry in θ encountered in the increasing frequency scale) are divided into two types: 1) the EH_{n1} modes, the cutoff structure of which is TE_{n1}, coaxial for any geometrical parameters of the structure; 2) the $EH_{nq}(q > 1)$ modes, the cutoff structure of which is TM or TE, according to the value of p. If we take p as the abscissa and $y = kb$ as the ordinate of Cartesian axes, the curves representing the cutoff frequencies of the TM_{nq} modes are straight lines parallel to the p axis, intersecting the y axis at y_n^i; the straight lines $y = px_n^j$ having a slope x_n^j represent the cutoff frequencies of the TE_{nj} modes; the curves $y = z_n^v p$ represent the cutoff frequencies of the TE_{nv} coaxial modes. We have plotted these curves in Fig. 3 for $n = 1$ and $i,j,v = 1 \cdots 4$. As p varies from ∞ to 1, the curve that represents the variation of the qth (>1) cutoff frequency is a continuous step function. This is shown in Fig. 3 by the double and triple arrows for the second and third cutoff frequencies of the modes symmetric in θ The exchange of cutoff frequencies is explained by the coupling between modes of the same θ symmetry. Such two EH modes are not orthogonal and are coupled according to the theory of Pierce and Tien [10]. For a given value, $p = p_0$, the order of the cutoff frequencies is determined by noting the ordinates of the points of intersection of the line $p = p_0$ with the curves in the order of increasing values of y.

C. Properties of Hybrid Modes

The asymptotic values ($\beta \to \infty$) of the dispersion relation show the different properties of these hybrid modes.

1) EH_{n1} Modes: These modes can be slow, fast, or can travel at light velocity according to the frequency. Their dispersion curves tend asymptotically to the straight line

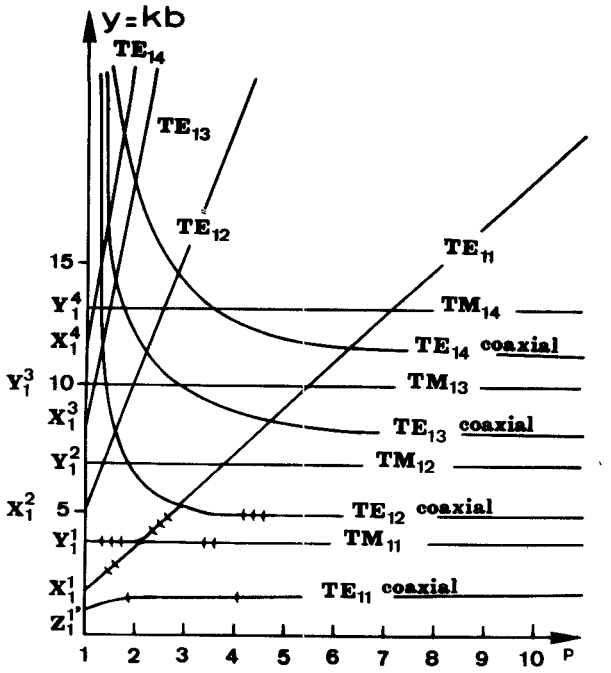

Fig. 3. The cutoff frequencies of the EH modes with first-order angular symmetry as a function of $p = b/a$.

$ka = n$ and pass through a maximum $(ka)_{max} = n + \Delta_n$, where Δ_n is a very small positive number ($\Delta_1 \simeq 0.017$).

The relations (8) and (9) show that for any value of p the ordinate of the intersect point from the dispersion curve to the straight line $v_p = c$ exists only in the range $(n^2 - 1)^{1/2} \leq ka \leq n$. The maximum ordinate, always greater than n, is in the domain of the slow waves.

At $v_p < c$, the properties of EH_{n1} modes are the same as those of the modes of the open ring line investigated by Sensiper [2]. If we substitute the modified Bessel functions to the hyperbolic Bessel functions of the first and second kinds in (7) and allow b to tend to infinity we obtain the following dispersion relation:

$$\frac{\beta^2}{k^2} = -\left(\frac{k_c{}^*a}{n}\right)^2 \cdot \frac{I_n'(k_c{}^*a)}{I_n(k_c{}^*a)} \cdot \frac{K_n'(k_c{}^*a)}{K_n(k_c{}^*a)}$$

where $k_c{}^{*2} = \beta^2 - k^2$. This expression is the same as that obtained by Sensiper for the open ring line.

The transverse components of the electromagnetic field deduced from (3) and (4) are indeterminate at $v_p = c$. After transformations [9], we obtain the proper components (see the Appendix) and express the power for the fundamental EH_{11} mode by

$$P = E^{II^2} \frac{\pi a^2}{2Z} \left[(ka)^2 p^2 \left\{ \log p + \frac{5}{6}p^2 - \frac{1}{4} - \frac{1}{2p^2} - \frac{1}{12p^4} \right\} + 1 - \frac{5}{4}p^2 + \frac{1}{4p^2} - p^2 \log p + \frac{1}{2}\frac{(p^2-1)^2}{p^2} \left\{ \frac{(ka)^2}{3} - 1 \right\} \right].$$

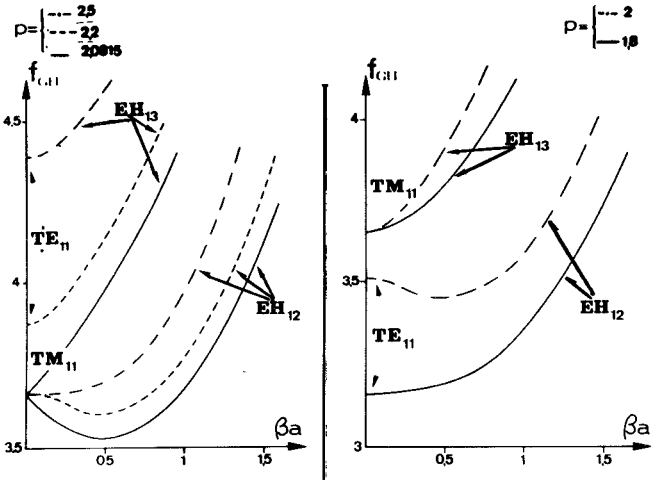

Fig. 4. Dispersion characteristic of the EH_{12} and EH_{13} modes as p decreases from 2.2 to 1.8 with $2b = 0.1$ m.

This power flux is always positive and brings into evidence that this mode is forward at $v_p = c$.

2) *EH_{nq} ($q > 1$) Modes:* The dispersion curves of these modes are asymptotic to the straight line $v_p = c$ when ω tends to infinity. Consequently, the EH_{nq} modes are fast modes.

When p is varied, all these hybrid modes with $n\theta$ symmetry present successively an abnormal dispersion curve with a minimum and exchange the cutoff frequencies for particular values of p.

Fig. 4 shows how the dispersion curves of the EH_{12} (TM_{11} at cutoff) and EH_{13} (TE_{11} at cutoff) modes change as p decreases from 2.2 to 1.8.

On both sides of $p = 2.08$, for which the cutoff frequencies of the EH_{12} and EH_{13} modes are equal to each other, the characteristic of the EH_{12} mode is distorted, having a minimum beyond cutoff in the fast-wave domain ($v_p > c$). This point is the upper boundary of a frequency zone in which the wavenumber is complex, even though there are no losses in walls or medium [5], [11]. For all values of p below 2.08 the cutoff structure of the EH_{12} mode is TE_{11}, whereas that of the EH_{13} mode is TM_{11}.

Fig. 5 shows the theoretical dispersion curves of the modes of the shielded ring line for the following geometrical parameters: $2b = 10$ cm, $2a = 5$ cm.

V. Experimental Results

In the real periodic structure, a progressive mode is constituted of an infinite number of spatial harmonics; their wavenumbers are of the form $\beta_m = \beta_0 + 2\pi m/H$, in which $\beta_0 = \omega/v_{p0}$ is the wavenumber of the fundamental component of the modes. The dispersion curve is an even periodic curve with periodicity $2\pi/H$. For recording the dispersion characteristics of the first modes, we transformed a section of the structure into a resonant cavity by placing shorting end plates in two symmetry planes midway between the rings.

In this cavity three equally spaced rods of sintered alumina hold up and adjust the rings. Between the rings,

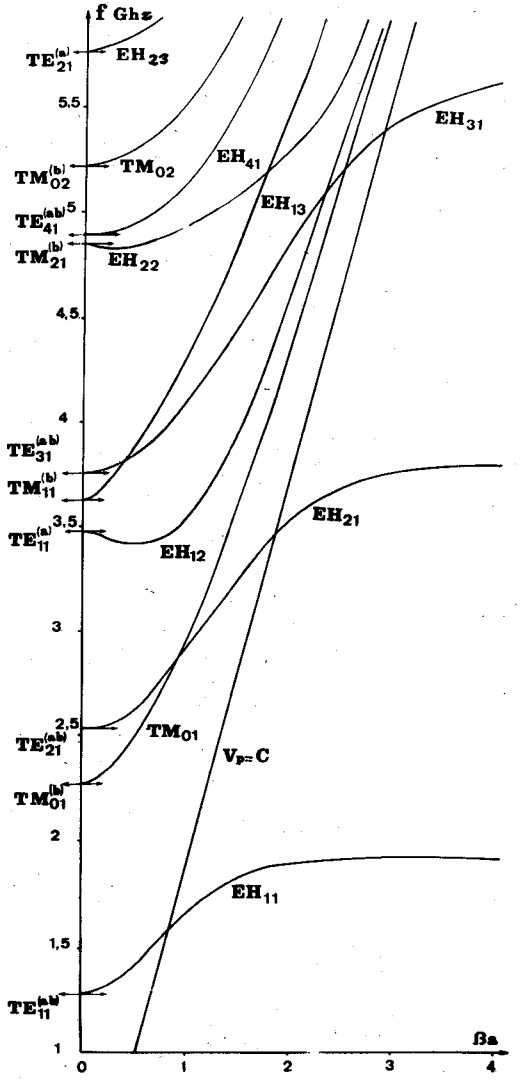

Fig. 5. Theoretical dispersion curves for the first modes of a shielded ring line ($2b = 0.1$ m, $p = b/a = 2$).

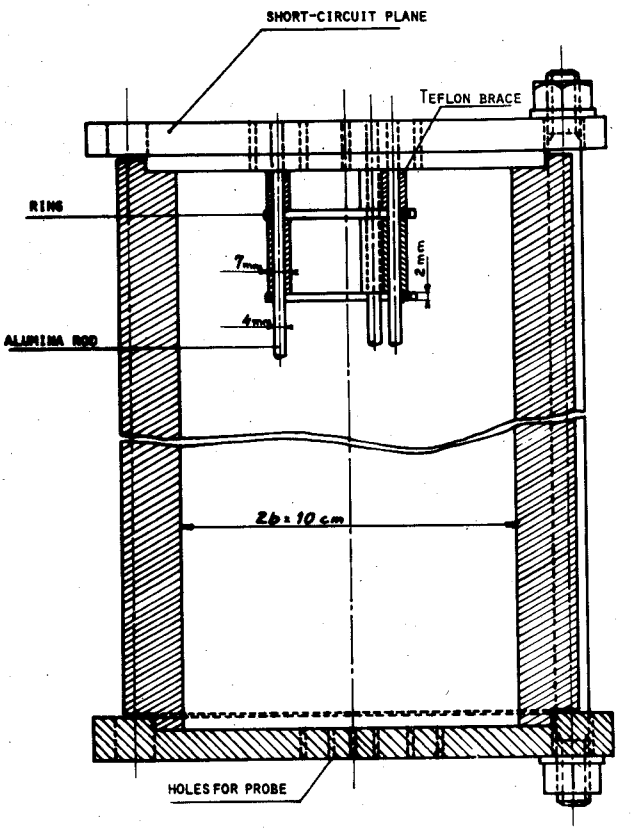

Fig. 6. Experimental cavity.

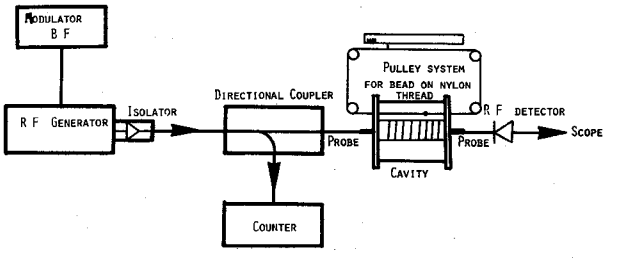

Fig. 7. Schematic diagram of the experimental setup.

Teflon braces are threaded on the rods and keep the constant period (Fig. 6). A series of holes was drilled in the short-circuit planes, allowing us to investigate the r and θ variation of the modes with the aid of electric and magnetic probes connected to detectors. Once the symmetry of the mode has been established and the resonant frequency measured with an electronic counter, it is convenient to measure the phase difference $\beta_0 L$ of the fields over the length $L = nH$ to enable us to measure the corresponding point of the dispersion characteristic in the Brillouin diagram. In order to make this measurement, we explore the system of standing waves in the structure by moving a dielectric bead parallel to the z axis (Fig. 7); this perturbs the resonant frequency by an amount proportional to the square of the E-field.

Figs. 8 and 9 show the results of measurements on the structures having the same diameters $2b = 10$ cm and $2a = 42$ mm, with pitches equal to 10 mm and 25 mm. Beside these curves are indicated the theoretical values of the cutoff frequencies of the roots at $v_p = c$ and the asymptotic values of the frequency for the different modes. From these diagrams, we see that dispersion characteristics have just the appearance predicted by the theory.

The dispersion curves of the EH_{n1} modes are very flat in the slow-wave domain as theory predicts (see Fig. 5). The periodicity affects these curves and reduces their passbands as the pitch increases. When the phase velocity is equal to the velocity of light, the experimental frequencies of the EH_{11} and EH_{21} modes should be higher than the theoretical values which are obtained by the sheath theory. Now, they are smaller for the structure of pitch 10 mm. This departure caused by the alumina rods which slightly lowers the resonant frequencies of the cavity.

The agreement is good for the coupling of the EH_{12} and EH_{13} modes, but the increase in spacing causes a certain delay because the experimental cutoff frequency is lower than the theoretical value which is that of a TE_{11}

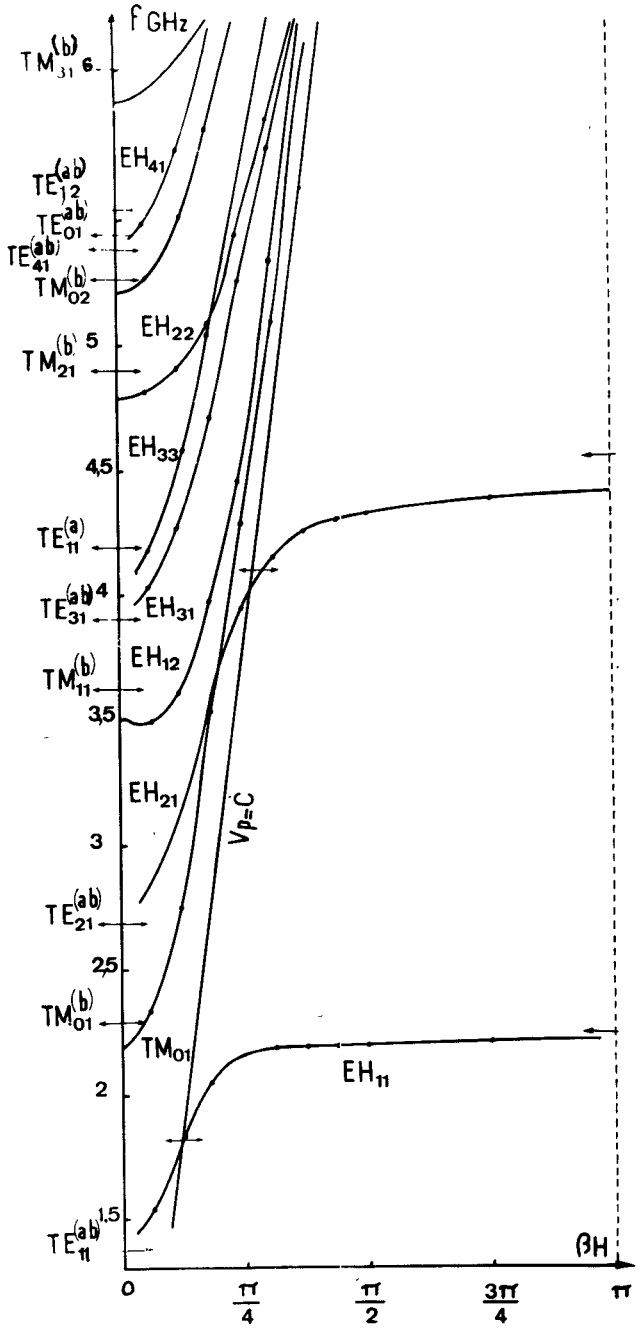

Fig. 8. Dispersion characteristic for the fundamental components of the mode of a shielded ring line (H = 0.01 m, $2a$ = 0.042 m, $2b$ = 0.1 m, $p = b/a$ = 2.38).

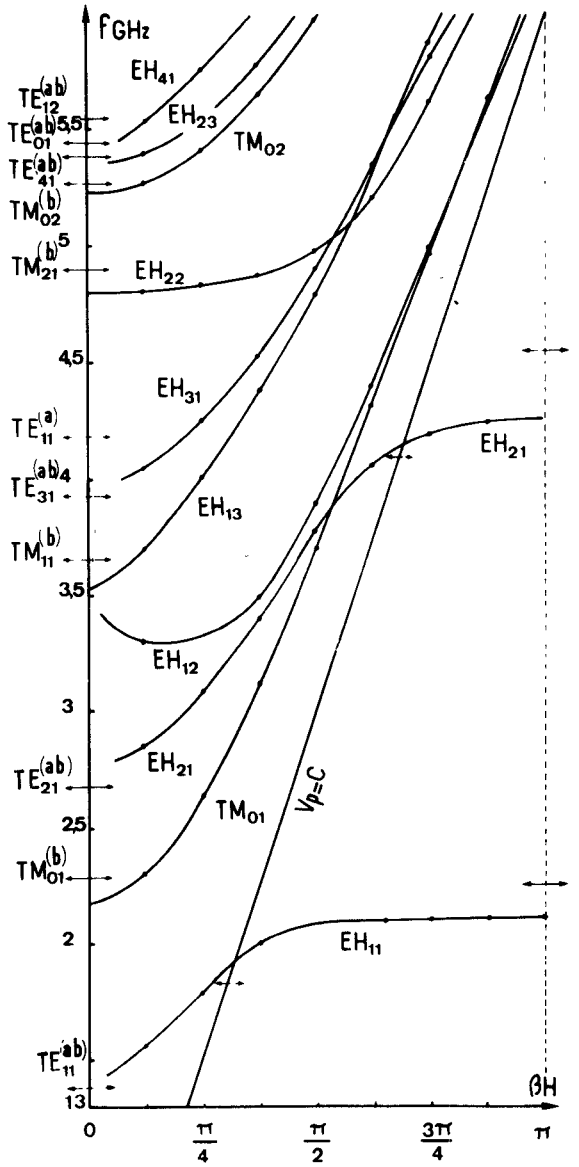

Fig. 9. Dispersion characteristic for the fundamental components of the mode of a shielded ring line (H = 0.025 m, $2a$ = 0.042 m, $2b$ = 0.1 m, $p = b/a$ = 2.38).

mode in a smooth guide of diameter $2a$. For H = 25 mm, the discrepancy between the theoretical and experimental values is much higher than in the case H = 10 mm. This is explained by the fact that as the pitch increases, the interaction between the rings is reduced; so that to obtain the same degree of coupling, p must be smaller. For modes that reduce to TM modes at cutoff, the experimental frequencies are lowered both by rings and alumina rods.

Fig. 10 shows the results of measurements on the structure with spacing 25 mm and p = 1.62. The passband of the EH_{n1} modes has considerably lowered (as theory predicts) in comparison with Fig. 9. We notice the cutoff frequency exchange between the EH_{22} and EH_{23} modes.

VI. Conclusion

This theoretical and experimental analysis provides detailed knowledge on the propagation of electromagnetic waves into the shielded ring line. The EH_{n1} modes which present a finite passband determined by the geometrical parameters of the structure can interact with particles traveling at velocities close to the light velocity. For deflecting RF structures, the fundamental EH_{11} mode is the only interesting one, because its gradient of longitudinal electric component is different from zero on the axis of the structure.

We have carried out studies on a shielded ring waveguide operating in the EH_{11} deflector mode with a phase difference $\beta H = \pi/2$ across a cell at $v_p = c$. Two Teflon

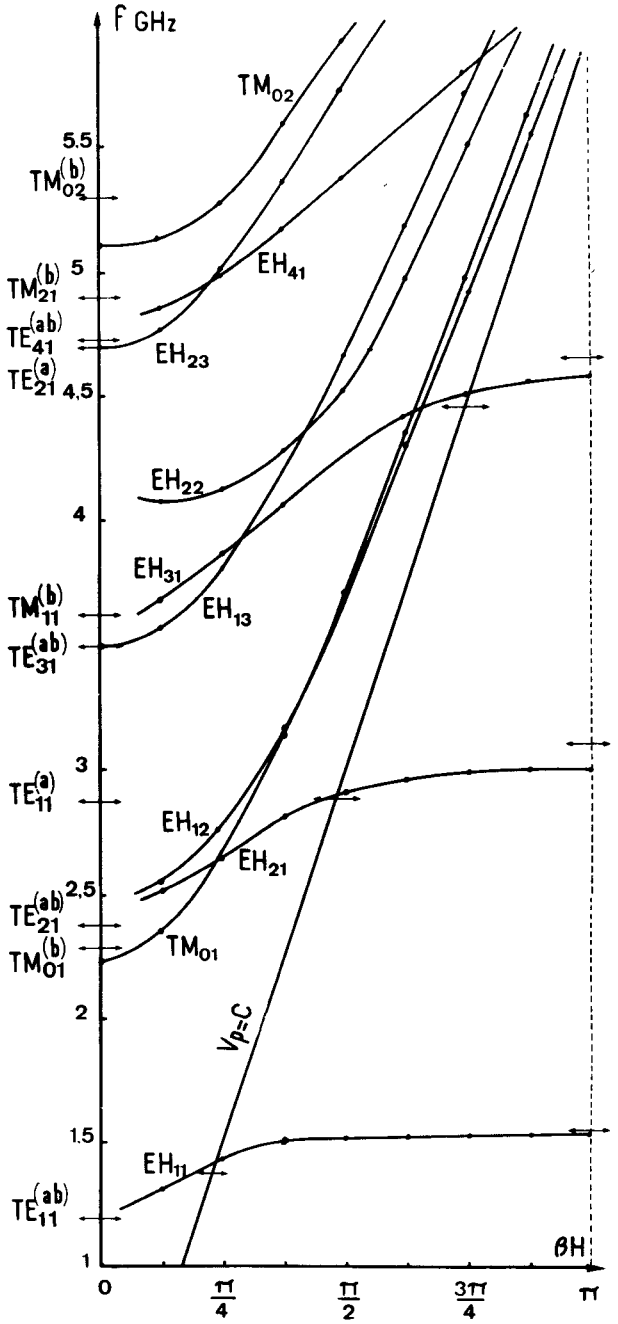

Fig. 10. Dispersion characteristic for the fundamental components of the mode of a shielded ring line (H = 0.025 m, $2a$ =0.062 m, $2b$ = 0.1 m, $p = b/a = 1.62$).

supports replace the alumina rods and are set in a plane where the longitudinal electric component is zero. At 3 GHz, the deflection constant for a such guide is $E_0/P^{1/2} = 1.23 \cdot 10^3$ V/W$^{1/2}$, with a group velocity $v_g = 7 \cdot 10^7$ m/s, where E_0 is the amplitude of E_z and P the power flux. For the deflecting disk-loaded waveguide in operation at CERN this constant is equal to $E_0/P^{1/2} = 1.88 \cdot 10^3$ V/W$^{1/2}$, with a group velocity $v_g = 7.2 \cdot 10^6$ m/s and a working frequency 2.855 GHz [12].

Our structure, as it stands, has lower deflecting properties. We believe these can be strongly improved by investigating the influence of the geometrical parameters of the structure and the ring shape in order to reduce the space harmonics. Their amplitude is not negligible. An important advantage of the deflecting ring waveguide is that the diameter is about half as large as that of the deflecting disk-loaded waveguide working at the same frequency. This property is particularly interesting in the construction of a deflecting guide for heavy particles at low frequency.

Appendix

Components of the Electromagnetic Field at $v_p = C$

A. Axial Zone

$$E_z^{I} = E\rho^n \cos n\theta$$

$$Z_0 H_z^{I} = -E\rho^n \sin n\theta$$

$$E_r^{I} = -j \frac{E}{2(n+1)} \rho^{n-1}\{(ka)^2 + \rho^2\} \cos n\theta$$

$$E_\theta^{I} = -j \frac{E}{2(n+1)} \rho^{n-1}\{(ka)^2 - \rho^2\} \sin n\theta$$

$$Z_0 H_r^{I} = j \frac{E}{2(n+1)} \rho^{n-1}\{(ka)^2 - \rho^2 - 2n(n+1)\} \sin n\theta$$

$$Z_0 H_\theta^{I} = j \frac{E}{2(n+1)} \rho^{n-1}\{(ka)^2 + \rho^2 - 2n(n+1)\} \cos n\theta$$

with $E = E^{I}/2^n n!$.

B. Coaxial Zone

$$E_z^{II} = \frac{E^{II}}{n} \left\{ \left(\frac{\rho}{kb}\right)^n - \left(\frac{kb}{\rho}\right)^n \right\} \cos n\theta$$

$$Z_0 H_z^{II} = -\frac{E^{II}}{nkb} \left\{ \left(\frac{\rho}{kb}\right)^n + \left(\frac{kb}{\rho}\right)^n \right\} \sin n\theta$$

for $n = 1$

$$E_r^{II} = jE^{II} \left\{ \frac{\rho^2}{4kb} - \frac{P_1}{\rho^2} + kb \log \frac{kb}{\rho} - Q_1 \right\} \cos\theta$$

$$E_\theta^{II} = jE^{II} \left\{ \frac{\rho^2}{4kb} - \frac{P_1}{\rho^2} - kb \log \frac{kb}{\rho} + Q_1 \right\} \sin\theta$$

$$Z_z H_r^{II} = -jE^{II} \left\{ \frac{\rho^2}{4kb} - \frac{R_1}{\rho^2} - kb \log \frac{kb}{\rho} + S_1 \right\} \sin\theta$$

$$Z_0 H_\theta^{II} = jE^{II} \left\{ \frac{\rho^2}{4kb} - \frac{R_1}{\rho^2} + kb \log \frac{kb}{\rho} - S_1 \right\} \cos\theta$$

with

$$P_1 = (kb)^3 \left\{ \frac{\log p}{1 - p^2} - \frac{1}{4p^2} \right\}$$

$$Q_1 = (kb)\left\{\frac{\log p}{1-p^2} - \frac{1+p^{-2}}{4}\right\}$$

$$R_1 = kb + P_1$$

$$S_1 = \frac{1}{kb} + Q_1$$

for $n \geq 2$

$$E_r^{II} = -j\frac{E^{II}}{2n}\left\{\frac{\rho^{n-1}}{(ka)^n}(P_n - \rho^2 Q_n) + \frac{(ka)^n}{\rho^{n+1}}(R_n - \rho^2 S_n)\right\}\cos n\theta$$

$$E_\theta^{II} = j\frac{E^{II}}{2n}\left\{\frac{\rho^{n-1}}{(ka)^n}(P_n + \rho^2 Q_n) - \frac{(ka)^n}{\rho^{n+1}}(R_n + \rho^2 S_n)\right\}\sin n\theta$$

$$Z_0 H_r^{II} = -j\frac{E^{II}}{2n}\left\{\frac{\rho^{n-1}}{(ka)^n}(P_n + 2n\rho^{-n} + \rho^2 Q_n) - \frac{(ka)^n}{\rho^{n+1}}(R_n + 2n\rho^n + \rho^2 S_n)\right\}\sin n\theta$$

$$Z_0 H_\theta^{II} = -j\frac{E^{II}}{2n}\left\{\frac{\rho^{n-1}}{(ka)^n}(P_n + 2n\rho^{-n} - \rho^2 Q_n) + \frac{(ka)^n}{\rho^{n+1}}(R_n + 2n\rho^n - \rho^2 S_n)\right\}\cos n\theta$$

with

$$P_n = \frac{1}{p^{-n} - p^n}\left\{(ka)^2\left(\frac{1}{n-1} - \frac{p^{-2n}}{n+1}\right) - \frac{2(kb)^2}{n^2-1}\right\}$$

$$R_n = \frac{1}{p^{-n} - p^n}\left\{(ka)^2\left(\frac{p^{2n}}{n-1} - \frac{1}{n+1}\right) - \frac{2(kb)^2}{n^2-1}\right\}$$

$$Q_n = \frac{p^{-n}}{n+1} \qquad S_n = \frac{p^n}{n-1}.$$

References

[1] J. R. Pierce and L. M. Field, "Traveling-wave tubes," *Proc. IRE*, vol. 35, pp. 108–111, Feb. 1947.
[2] S. Sensiper, "Electromagnetic wave propagation on helical conductors," M.I.T. Res. Lab. Electron., Cambridge, Mass., Rep. 194, May 1951.
[3] J. Falnes, "Hybrid modes of a circular cylindrical cavity containing a unidirectionally conducting coaxial sheet," in *Electromagnetic Theory and Antennas*, pt. 2, E. C. Jordan, Ed. New York: Pergamon, 1962, pp. 941–950.
[4] G. Goudet and P. Chavance, *Ondes Centimétriques*, 1955, p. 73.
[5] Y. Garault, "Hybrid EH guided waves," in *Advances in Microwaves*, vol. 5, L. Young, Ed. New York: Academic, 1970.
[6] Y. Garault and J. P. Fenelon, "Hybrid waves in the through periodic waveguide," *C. R. Acad. Sci.*, vol. 567, pp. 540–543, 1968.
[7] H. Hahn, "The deflecting mode in the circular iris-loaded waveguide of an RF particle separator," Brookhaven Nat. Lab., Brookhaven, N.Y., BNL-AGS Internal Rep. HH-5, 1962.
[8] H. Hahn and H. J. Halama, "Mode identification in the iris-loaded waveguide of an RF particle separator," Brookhaven Nat. Lab., Brookhaven, N.Y., BNL-AGS Internal Rep. HH/HJH-2, 1963.
[9] C. Fray, "La ligne à anneaux blindée," Thèse de 3 ème cycle, Faculty Sciences, Univ. Poitiers, Poitiers, France, May 1970.
[10] J. R. Pierce and P. K. Tien, "Coupling of modes in helixes," *Proc. IRE*, vol. 42, pp. 1389–1396, Sept. 1954.
[11] V. Vaghin, "Etude des ondes électromagnétiques hybrides dans les structures cylindriques. Application des résultats aux modes déflecteurs," CERN Rep. 71-4.
[12] P. H. Bernard, H. Lengeler, and V. Vaghin, "New disk-loaded waveguide for the CERN separator," CERN Rep. 70-26, Sept. 17, 1970.

Resonance Conditions of Open Resonators at Microwave Frequencies

TATSUO ITOH, MEMBER, IEEE, AND RAJ MITTRA, FELLOW, IEEE

Abstract—**This paper presents an extension of Vajnshtejn's approach for computing the resonance frequencies and loss factors of Fabry–Perot (FP) resonators at microwave frequencies. Numerical results are presented for FP resonators operated at microwave through millimeter frequency range.**

Manuscript received March 28, 1973; revised September 14, 1973. This work was supported in part by the Dikewood Corporation Subcontract DC-SC-72-19 for the Air Force Special Weapons Center, Prime Contract Number F29601-72-C-0087, and in part by the U.S. Army Research Grant DA-ARO-D-31-124-G77.

The authors are with the Department of Electrical Engineering, University of Illinois, Urbana, Ill. 61801.

I. Introduction

FABRY–PEROT (FP) and other types of open resonators find useful applications at optical as well as millimeter or microwave frequencies. Typically, these resonators consist of two plane or curved mirrors facing